Enhanced fatty acid scavenging and glycerophospholipid metabolism accompanies melanocyte neoplasia progression in zebrafish

Fiona Henderson[1,2,*], Hannah R. Johnston[3,*], Andrew P. Badrock[3,*], Emrys A. Jones[4], Duncan Forster[1], Raghavendar T. Nagaraju[3], Christos Evangelou[3], Jivko Kamarashev[5], Michael Green[1], Michael Fairclough,[1] Irene Barinaga-Rementeria Ramirez[3], Shuning He[6,7], B. Ewa Snaar-Jagalska[6], Katherine Hollywood[8], Warwick B. Dunn[8,9], Herman P. Spaink[6], Michael P. Smith[3], Paul Lorigan[10], Emmanuelle Claude[4], Kaye J. Williams[2,$], Adam W. McMahon[1,$,&] , Adam Hurlstone[3,$,&]

[1]Wolfson Molecular Imaging Centre, Division of Informatics, Imaging and Data Sciences, School of Health Sciences, Faculty of Biology, Medicine and Health, The University of Manchester, Manchester Academic Health Science Centre, Manchester, M20 3LJ, UK

[2]Division of Pharmacy and Optometry, School of Health Sciences, Faculty of Biology, Medicine and Health, The University of Manchester, Manchester Academic Health Science Centre, Stopford Building, Manchester, M13 9PT, UK

[3]Division of Cancer Sciences, School of Medical Sciences, Faculty of Biology, Medicine and Health, The University of Manchester, Manchester Academic Health Science Centre, Michael Smith Building, Manchester, M13 9PT, UK

[4]Waters Corporation, Wilmslow, SK9 4AX, UK

[5]Department of Dermatology and Allergy, UniversitätsSpital Zürich, Gloriastraße 31, 8091 Zürich, Switzerland

[6]Institute of Biology, Leiden University, Gorlaeus Laboratory, Einsteinweg 55, 2333 CC Leiden, The Netherlands

[7]Current affiliation: Department of Pediatric Oncology, Dana-Farber Cancer Institute, Harvard Medical School, Mayer Building 630, 450 Brookline Ave, Boston, MA, 02115

[8]Centre for Advanced Discovery and Experimental Therapeutics (CADET), Central Manchester University Hospitals NHS Foundation Trust, Manchester, M13 9WL, UK

[9]Current affiliation: School of Biosciences, Institute of Metabolism and Systems Research and Phenome Centre, University of Birmingham, Edgbaston, Birmingham, B15 2TT, UK

[10]Division of Cancer Sciences, School of Medical Sciences, Faculty of Biology, Medicine and Health, The University of Manchester and Department of Medical Oncology, The Christie NHS Foundation Trust, Wilmslow Road, Withington, Manchester M20 4BX, UK

*contributed equally to this paper; [$]co-senior authors

[&]correspondence to:

Dr Adam Hurlstone, Michael Smith Building, The University of Manchester, Dover Street, Manchester M13 9PT, UK; phone: +44 (0) 161 275 1574; email: adam.hurlstone@manchester.ac.uk (Lead contact)

Dr Adam McMahon, Wolfson Molecular Imaging Centre, The University of Manchester, 27 Palatine Road Withington Manchester M20 3LJ, UK; phone: +44 (0) 161 275 0026; email: adam.mcmahon@manchester.ac.uk

Running title: Fatty acid uptake in zebrafish melanocyte neoplasia

Disclosure of Potential Conflicts of Interest: No potential conflicts of interest were disclosed.

Abstract

Alterations in lipid metabolism in cancer cells impact cell structure, signaling, and energy metabolism, making lipid metabolism a potential diagnostic marker and therapeutic target. In this study, we combined positron emission tomography (PET), desorption electrospray ionisation-mass spectrometry (DESI-MS), non-imaging MS, and transcriptomic analyses to interrogate changes in lipid metabolism in a transgenic zebrafish model of oncogenic RAS-driven melanocyte neoplasia progression. Exogenous fatty acid uptake was detected in melanoma tumor nodules by PET using the palmitic acid surrogate tracer 14(R,S)-18F-fluoro-6-thia-heptadecanoic acid ([18F]-FTHA), consistent with upregulation of genes associated with fatty acid uptake found through microarray analysis. DESI-MS imaging revealed that FTHA uptake in tumors was heterogeneous. Transcriptome and lipidome analyses further highlighted dysregulation of glycerophospholipid pathways in melanoma tumour nodules, including increased abundance of phosphatidyl ethanolamine and phosphatidyl choline species, corroborated by DESI-MS which again revealed heterogeneous phospholipid composition in tumors. Overexpression of the gene encoding lipoprotein lipase (LPL), which was upregulated in zebrafish melanocyte tumor nodules and expressed in the majority of human melanomas, accelerated progression of oncogenic RAS-driven melanocyte neoplasia in zebrafish. Depletion or antagonism of LPL suppressed human melanoma cell growth; this required simultaneous fatty acid synthase (FASN) inhibition when FASN expression was also elevated. Collectively, our findings implicate fatty acid acquisition as a possible therapeutic target in melanoma, and the methods we developed for monitoring fatty acid uptake have potential for diagnosis, patient stratification, and monitoring pharmacological response.

Significance: Findings demonstrate the translational potential of monitoring fatty acid uptake and identify lipoprotein lipase as a potential therapeutic target in melanoma.

Keywords: Mass Spectrometry Imaging, Lipid Metabolism, Transcriptome Analysis, LPL, Fatty Acid

Introduction

Since Otto Warburg's pioneering work, it has been recognised that cancer cells undergo metabolic changes to sustain their unbridled growth and dissemination. Lipids are major cell membrane components, signalling molecules, and also an energy source for cells. Altered lipid metabolism is essential for cancer progression, with lipids playing a key role in cancer cell proliferation and metastasis. Moreover, lipidomics is generating insight into disease mechanisms and identifying new therapeutic targets (1). While still sparse, emerging evidence implicates altered lipid metabolism in the development of melanoma too, with alterations in the lipidome differentiating benign skin neoplasms from melanoma (2).

Fatty acids are building blocks for complex lipids incorporated into membranes as well as substrates for β-oxidation, a major energy yielding reaction. How cancer cells obtain fatty acids is altered compared to healthy tissue, although the exact mechanisms remain to be elucidated. Fatty acids can be synthesized *de novo* by the enzyme fatty acid synthase (FASN). FASN is overexpressed in several cancers including melanoma (3, 4) and has been the target of drug development programs over decades (5). While FASN inhibitors can antagonise the proliferation of cancer cell lines including melanoma cell lines (6, 7), they have failed in the clinic due to insufficient efficacy and excessive toxicity (5). Fatty acids can also be scavenged from the blood supply, or potentially acquired through close contact with adipocytes (8, 9). Fatty acid scavenging by fatty acid binding protein 7 (FABP7) has been associated with enhanced proliferation and invasive capability of melanoma cells (10-12), while CD36-mediated fatty acid scavenging is prominent in metastasis-initiating melanoma cells (13). Further, it was recently shown that FATP1/SLC27A1, which transports long-chain fatty acids into cells, is enriched in melanoma compared to other cancer types (9), thereby highlighting the importance of fatty acid uptake for melanoma progression.

The small domesticated fish, *Xiphophorus*, medaka and zebrafish, have been used for modelling melanoma since (in the case of *Xiphophorus*) the early decades of the last century. Melanocyte tumours arising in these models show comparable histopathology and molecular signatures to human melanoma due to the conservation of skin structures, melanocyte development, and signalling pathways controlling cell growth and invasion, all underpinned by the extensive conservation of vertebrate genomes (14). Previously, we have used transgenic zebrafish to establish a critical role for ERK MAPK in initiating melanocyte neoplasia and both PI3K and RAC in its malignant progression (15, 16). More recently, transgenic zebrafish were used to reveal cooperation between FATP1 and $BRAF^{V600E}$ in stimulating melanocyte neoplasia, while melanoma cell transplantation into zebrafish revealed preferential metastasis to adipose tissue (9).

Positron emission tomography (PET) is a highly sensitive *in vivo* imaging technique for visualising non-invasively in 3D the distribution of an administered radiolabelled pharmaceutical (or tracer). Fluorodeoxyglucose-PET which detects glucose uptake capacity has become a well-established technique to visualise tumour locations. However, there have been relatively few PET-based studies investigating the role of lipid metabolism in cancer. PET tracers such as [^{11}C]-choline and [^{11}C]-acetate have emerged as useful tracers to study lipogenesis in tumours (17-20); but they cannot be used to investigate uptake of exogenous lipids. The tracer 14(R,S)-(18)F-fluoro-6-thia-heptadecanoic acid (herein [^{18}F]-FTHA), an analogue of palmitic acid (a saturated fatty acid with a 16 carbon chain) has previously been used to study free fatty acid uptake in tissues (21) but has not yet been used to investigate fatty acid uptake in tumours.

Tumours are not uniform, and this spatial heterogeneity complicates the study of metabolism. Tumour heterogeneity also poses a major problem for therapy, particularly when the disease progresses to the metastatic stage. PET is able to image metabolic heterogeneity *in vivo* somewhat, however it is limited by low spatial resolution— in the low millimetre range, but exact resolutions vary depending on the scanner model and radioisotope used— and its targeted nature (defined by the tracer used). In contrast to PET, desorption electrospray ionisation mass spectrometry (DESI-MS) imaging is an ambient *ex vivo* technique in which a stream of charged microdroplets is directed onto a tissue section in order to generate gaseous ions from species on the section surface. These ions are then taken up into a mass spectrometer inlet for analysis. Fatty acids and phospholipids ionise well by DESI-MS, making it an ideal lipid imaging tool (22). DESI-MS has the advantage of being an untargeted label-free technique, revealing the distribution of large numbers of lipids within a tissue section in one analysis at higher spatial resolution than achievable by PET (< 100 μm). Further, tandem mass spectrometry (DESI-MS/MS) can be performed post-imaging to identify individual lipid species.

Here, transcriptome profiling and non-imaging mass-spectrometry based metabolomics have been combined with PET and DESI-MS imaging modalities to investigate fatty acid uptake and lipid metabolism in oncogenic RAS-driven zebrafish melanocyte neoplasia. Transcriptome profiling identified a gene expression program associated with disease progression, which included genes involved in fatty acid uptake and glycerophospholipid metabolism. Enhanced fatty acid uptake was confirmed by both PET and DESI-MS imaging of FTHA. DESI-MS and conventional mass spectrometry also confirmed enhanced glycerophospholipid metabolism. DESI-MS provided insight into tumour heterogeneity in lipid metabolism. The product of one disease progression associated gene, lipoprotein lipase (LPL), implicated in fatty acid scavenging (23), was found to be expressed in a majority of human melanoma cell lines and tumour samples.

LPL depletion or antagonism suppressed melanoma cell growth, although high concurrent FASN expression could compensate for reduced LPL activity.

Materials and methods

Zebrafish genetic models

All regulated procedures involving zebrafish were ethically approved by The University of Manchester Animal Welfare and Ethical Review Body (AWERB) and carried out under licence in accordance with the UK Home Office Animals (Scientific Procedures) Act (1986), the guidelines of the Committee of the National Cancer Research Institute and the University's Policy on the Use of Animals in Research. Zebrafish were housed at the Biological Services Unit (BSU) at The University of Manchester at ~28 °C under a 14 hours light/10 hours dark cycle. Transgenic zebrafish expressing $BRAF^{V600E}$ or $HRAS^{G12V}$ in the melanocyte lineage have been previously described (15). Generation of the $NRAS^{G12D}$ construct was previously described (24) and breeding from founders resulted in the creation of a transgenic line. The $HRAS^{G12V}$ or $NRAS^{G12D}$ lines were crossed onto a *mitfa*$^{w2/w2}$ (*mitfa*$^{-/-}$) background to suppress melanocyte development and the $NRAS^{G12D}$ transgene further onto a *tp53*$^{M214K/M214K}$ background to promote tumourigenesis. Melanocyte restoration and simultaneous overexpression of LPL, CCND1, mCherry or eGFP were then achieved by injection of embryos with a mitfa-minigene containing plasmid as previously described (25). Briefly, mCherry cDNA amplified from a vector and LPL cDNA amplified from zebrafish tumours using primers below were cloned into pDONR221 using Gateway assembly (Gateway cloning kit, Thermo Scientific) to create pME mCherry and pME LPL. These were then incorporated into the mitfa-minigene containing destination vector together with p5'E *mitfa* promoter and p3'E-polyA by Gateway cloning. The p5'E *mitfa* promoter, and p3'E-polyA entry clones as well as the destination vector and CCND1 and eGFP control expression plasmids were kindly provided by Dr. Craig Ceol (UMass Medical School). Expression plasmid was injected into zebrafish zygotes along with Tol2 mRNA. pCS2-TP plasmid for Tol2 mRNA generation was a kind gift from Dr. Koichi Kawakami (National Institute of Genetics). Only zebrafish embryos with near complete melanocyte rescue at 5 days post-fertilisation (dpf) were retained and followed weekly for tumour development. Tumour nodules arising on fins, where the full mass could be evaluated, were measured in two directions using calipers (Expert Dual Reading Ip65 Digital Vernier Caliper 46611, Draper) when they were first detected and again two weeks later to determine growth rate. The cross-sectional area (A) was calculated using the formula π((d1+d2)/4)^2 and growth rate per week as $(A_{week2}-A_{week1})/2$. Animals were sacrificed before clinical symptoms arose.

Primers for mCherry and LPL amplification

mCherry	attB1F: GGGGACAAGTTTGTACAAAAAAGCAGGCTCGCCACCATGGTGAGCAAGGGCGAGGAGG attB2R: GGGGACCACTTTGTACAAGAAAGCTGGGTACCTTACTTGTACAGCTCGTCCATG
LPL	attB1F: GGGGACAAGTTTGTACAAAAAAGCAGGCTTCGCCACCATGATGTTTAATAAGGGGAGAG attB2R: GGGGACCACTTTGTACAAGAAAGCTGGGTACTTTACTCGTTGTTCTGTTTG

Transcriptome Analysis

The microarray slides, custom-designed by Agilent Technologies, have been described elsewhere (26) and the design submitted to the Gene Expression Omnibus (GEO) database (www.ncbi.nlm.nih.gov/geo) with accession number GPL7735. For RNA isolation, three pools of 10 caudal fins or three pools of 6 tumours within caudal fins were snap-frozen in liquid nitrogen and subsequently stored at -80 °C. Samples were homogenized in 1 ml of TRIzol reagent (Thermo Fisher Scientific), and subsequently total RNA was extracted according to the manufacturer's instructions. RNA samples were incubated for 20 minutes at 37 °C with 10 U of DNase I (Roche Applied Science) to remove residual genomic DNA before purification using the RNeasy MinElute Cleanup kit (Qiagen). The integrity of the RNA was confirmed by lab-on-chip analysis using the 2100 Bioanalyzer (Agilent Technologies). Samples used for microarray analysis had an average RNA integrity number value of 9 and a minimum RNA integrity number value of 8.

RNA labelling was performed as described elsewhere (26). For comparison, aRNA of wild-type fish were coupled with Cy3 and aRNA of transgenic lines were coupled with Cy5. Hybridization and scanning were performed according to standard Agilent protocols. The feature extraction software version 9.5, protocol ge2_V5_95 from Agilent was used to generate the feature extraction data. For the background subtraction the option 'No background subtraction and spatial detrend' was used. The arrays were scanned twice with 10% PMT and 100% PMT laser power and the XDR function was used to extend the dynamic range by 10-fold. Microarray data was imported into Rosetta Resolver 7.0 (Rosetta Biosoftware) and subjected to default ratio error modelling. Data analysis was performed for unigene clusters (Unigene Build 105) and significance cut-offs for the ratios of wild-type *vs.* a particular transgenic line were set at 2-fold change and $p \leq 10^{-5}$. The two-dimensional hierarchical cluster analysis was performed with Rosetta Resolver settings for agglomerative algorithm (average link) with cosine correlation. The microarray data discussed in this publication have been deposited in GEO with Series accession number GSE76791 (https://www.ncbi.nlm.nih.gov/geo/query/acc.cgi?acc=GSE76791).

Human orthologs of the differentially expressed genes were determined using BioDBnet (27) and BioMart (28). Gene Ontology (GO) enrichment analysis for the human orthologs was performed using PANTHER Overrepresentation Test (Fisher's Exact test, Bonferroni correction for multiple testing) through the Gene Ontology Consortium enrichment analysis platform (29). For the GO analysis, gene function and gene ontology terms were based on the PANTHER Classification System (GO Ontology database Released 2018-11-15) (doi: 10.1038/nprot.2013.092).

[^{18}F]-FTHA PET scanning

Production of [^{18}F]-FTHA was carried out via nucleophilic [^{18}F] fluorination of a benzyl-14-(R,S)-tosyloxy-6-thiaheptadecanonate precursor (ABX advanced biochemical compounds), based on the method by DeGrado et al. (30) and was fully automated on a TRACERlab FXFN radiochemistry system (GE Healthcare). Animals were not fed the evening prior to scanning (to limit background signal in the gut). Fish were immersed in 200ml of water containing 100 MBq of [^{18}F] FTHA for 2 hours. Animals were then anaesthetised with MS222 and placed in cuvettes (held in place with sponge) and cuvettes placed in falcon tubes filled with ice water. Static PET scans were then performed for 5 and 10 minutes on a pre-clinical PET scanner (Inveon, Siemens, Germany). Fish were culled immediately after scanning without recovery from anaesthetic, and flash-frozen in isopentane. PET images were reconstructed using the 3d-OSEM/MAP algorithm (4 OSEM3D iterations and no MAP iterations, with a resolution of 1mm). Images were visualised using Inveon Research Workplace software (Siemens, Germany). Regions of interest (ROIs) were drawn manually over tumours and the SUV_{mean} (an average of all voxels) was calculated. Normalisation was performed using the dose of [^{18}F]-FTHA (average dose was 4 MBq) and the weight of the fish (average weight was 0.5g) to give standardised uptake values.

DESI-MS imaging

Fish were immersed in 100 ml of water containing 0.5 mg of FTHA for 30 mins, culled, then flash frozen in isopentane. Fish were sectioned to 12 µm onto glass slides. Imaging experiments were carried out on a 2D DESI system (Prosolia, Indianapolis, USA) mounted on a Xevo-G2-XS quadrupole-time of flight (Q-TOF) (Waters Corporation, Wilmslow, UK). The solvent spray consisted of 95% methanol and 5% water. Spray conditions used were a flow rate of 2 µl/minutes (using a syringe pump from Harvard Apparatus, Inc., Holliston, MA), with a nebulising gas of nitrogen at 4 bar pressure. Typical positions of the sprayer were used (sprayer 1.5mm above surface, 6mm sprayer to capillary distance, 75˚ sprayer impact angle, 5˚ collection capillary angle). The source temperature was 100 ˚C and the capillary voltage was set between 4.82 and 5kV.

Images were acquired using a scan rate of 1-10 scans/second, and a mass range of 50-1200 Da. The spatial resolution varied from 40-200 µm. Images were processed and normalised to total ion current (TIC) using the High Definition Imaging (HDI) v1.4 (Waters, Wilmslow, UK). MS/MS experiments were carried out on a Xevo-G2-XS Q-TOF mass spectrometer using argon as the collision gas and a collision energy range of 20 V - 40 V. Spray conditions were the same as DESI imaging. Interpretation of spectra was carried out with the help of LIPID MAPS Lipidomics Gateway database (http://www.lipidmaps.org) (31).

Haematoxylin and eosin staining

Haematoxylin and eosin (H&E) staining was carried out on sections after DESI-MS imaging, and also on adjacent sections. Slides were immersed in xylene (Sigma-Aldrich, UK) for two minutes, and then transferred to industrial methylated spirit (Sigma-Aldrich, UK) for 4 x 2 minutes. Sections were then immersed in tap water followed by 3 minutes in Harris haematoxylin (Sigma-Aldrich, UK), a rinse in hot water, and a one second dip in eosin (Leica, UK). Slides were transferred to industrial methylated spirit for (4 x 2 minutes), then to xylene (4 x 2 minutes), and left to dry. Aqueous mounting media (Abcam, UK) was used to mount coverslips (VWR, UK) onto slides and left overnight to dry. Images were acquired using a [*20x/0.80 Plan Apo*] objective using the 3D Histech Pannoramic 250 Flash II slide scanner, and processed using Panoramic viewer (3D HISTECH, Hungary).

Nile Red staining

Nile Red (Sigma-Aldrich, UK) stock solution was prepared at 0.5 µg/mL in acetone. For staining the stock was diluted 1:1000 in 80% glycerol. Cryosections were allowed to defrost for 40 minutes at room temperature. Samples were briefly washed with distilled water before 100 µL of Nile Red was added to each slide. Samples were incubated for 5 minutes in the dark before being cover-slipped and immediately imaged. Images were acquired on an Olympus BX51 upright microscope using a 10x/ 0.30 Plan Fln objective using a Coolsnap ES camera (Photometrics) through MetaVue Software (Molecular Devices). Specific band pass filter sets for FITC and Texas Red were used to prevent bleed-through from one channel to the next. Images were then processed and analysed using ImageJ (http://rsb.info.nih.gov/ij).

Lipid extraction and mass spectrometry analysis of metabolic pathways

Wild-type and V12RAS fish skin and tumour nodules from V12RAS fish were pooled to a mass between 25–35 mg. At least 6 biological pools were gathered for each sample. Extraction of tissue metabolites was

performed as previously described by lysing tissue in a mixture of chloroform, methanol and water to separate polar (methanol/water phase) and non-polar (chloroform phase) metabolites. Non-polar fractions were dried under vacuum for 16 hours. Ultra-high performance liquid chromatography mass spectrometry (UHPLC-MS) analysis of the non-polar extracts was performed using an (Accela UHPLC system coupled to an Orbitrap Velos MS. Univariate statistical tests (mean ratio with confidence intervals, Mann-Whitney U-test) and multivariate principal component analysis (PCA) were applied in R. Metabolites were annotated applying the software PUTMEDID_LCMS (32); all metabolites were annotated to level 2 as defined in the reporting standards for chemical analysis constructed by the Metabolomics Standards Initiative (33).

Integrating Transcriptomic and Lipidomic Analyses with MetScape

The MetScape (34) plugin for Cytoscape was used for integration. The analysed transcriptome data and mass spectrometry data were entered with their respective fold-change and P-values. The gene data was added with the human homologue Entrez gene identifier; the metabolites were added with KEGG compound identifiers. All mapping was performed with unmodified, standard settings and MetScape workflow.

Cell culture and LPL depletion by siRNA

All human melanoma cell lines were maintained in DMEM with L-glutamine, pyruvate and sodium bicarbonate (Sigma-Aldrich) supplemented with 10% fetal bovine serum (Life Technologies) and 1% penicillin/streptomycin solution (Sigma-Aldrich). Cell lines were authenticated using STR analysis. Normal human melanocyte (NHM) cells (Life Technologies) were maintained in medium 254 (Life Technologies) supplemented with 1% human melanocyte growth supplement (HMGS) (Life Technologies). All cells were maintained under standard conditions at 37°C with 5% CO_2 and routinely screened for mycoplasma infection.

For LPL depletion, siRNA was purchased from Dharmacon (sequences below). All siRNAs were diluted to 20 µM in 5X siRNA resuspension buffer (GE Dharmacon). The cells were plated 24 hours prior to transfection in 6 well plates and at a cell number to allow the cells to be at 60% confluence (200,000 cells per well). Cells were transfected with 20 pmol of siRNA using the Lipofectamine RNAiMAX transfection reagent (Thermo Fisher Scientific) as instructed by the manufacturer. A non-targeting control was included in every experiment. Fresh media was added after 24 hours or cells were collected.

<u>siRNA sequences</u>

control siRNA	AAUAUAAUCACUAUCAGGUGC
LPL siRNA A	GGCCUCUGCUUGAGUUGUA
LPL siRNA B	CCUACAAAGUCUUCCAUUA

Drug Dose-Response Analysis and Survival Assays

For drug dose-responses assays, cells were plated in 96-well plates and treated with serial dilutions of GSK264220A (Tocris) and C75 (Sigma Aldrich) for 72h. Cell survival was quantified by fixing and staining cells with 0.5% crystal violet in 4% formaldehyde and then measuring the absorbance of the solubilized dye (in 2% SDS in PBS) at an optical density of 595nm.

RNA isolation and real-time qPCR analysis

RNA was isolated from cells using TRIzol (QIAGEN). cDNA was synthesized from RNA using the Omniscript reverse transcriptase kit (QIAGEN) according to the manufacturer's instructions. Amplification of specific PCR products was detected using an Agilent technologies Stratagene Mx3000P system, the SensiMix SYBR No-ROX Kit (Bioline) and the following cycling conditions: 95°C for 10 minutes and 40 cycles of 95°C for 30s, 55°C for 45s and 72°C for 45s. Primer efficiency was previously determined > 90% and < 110% and correlation (R^2) over three log concentrations > 0.97. Relative expression using beta-actin (ACTB) expression to normalise and normal human melanocytes as a common reference was calculated using the ΔΔCt approach.

Primers used for qPCR analysis:

LPL	F: GACACAGCTGAGGACACTTG R: TGGAGTCTGGTTCTCTCTTG
FASN	F: CTTCCGAGATTCCATCCTACGC R: TGGCAGTCAGGCTCACAAACG
CD36	F: GACCTGCTTATCCAGAAGAC R: TTGCTGCTGTTCATCATAC
FABP7	F: AGCTGACCAACAGTCAGAAC R: ATGTGCTGAGAGTCCTGATG
FATP1	F: AGTACAACTGCACGATCGTC R: GCAGTCATAGAGCACGTCAG
FATP2	F: AGTTGGTGCTGTTGGAAGAG R: ACCAGAAGTCCAACTTCACC

ACTB	F: GCAAGCAGGAGTATGACGAG R: CAAATAAAGCCATGCCAATC

LPL Immunofluorescence

Cells were plated onto UV-treated cover slips contained in 6 well plates, washed with 1x PBS and then placed in a 4% paraformaldehyde and 1X PBS solution for 30 minutes. Coverslips were then washed in 1x PBS and again in 1M glycine (Sigma Aldrich). Coverslips were then incubated in 0.1% TX100/PBS (Sigma Aldrich) solution for 4 minutes to permeabilise cells before being incubated with a 1:100 dilution of mouse A4 anti-LPL monoclonal (ab21356, Abcam) in 0.5 µg/mL BSA/TBST for 20 minutes. Following this, coverslips were washed three times in PBS and then incubated with a secondary antibody conjugated to CY3 for a further 20 minutes. Coverslips were then washed in PBS and incubated with Cy3-labelled secondary antibody for 2 hr at RT and mounted using DAPi containing vectashield. (Vectorshield Antifade with DAPI, Vector Laboratories). Slides were sealed with clear polish. Images were collected on a Olympus BX51 upright microscope using a 10x/ 0.30 Plan Fln objective and captured using a Coolsnap ES camera (Photometrics) through MetaVue Software (Molecular Devices). Specific band pass filter sets for DAPI and Cy3 were used. Images were then processed and analysed using ImageJ (http://rsb.info.nih.gov/ij).

Western blotting

Laemmli buffer was added to cells for 1 minute before the well was scraped with a cell scraper and the buffer was transferred to a 0.5 mL tube and sonicated (VibraCell X130PB, Sonics Materials) for 30 seconds at 20% amplitude. Samples were then boiled for 5 minutes before being loaded onto precast gels in the SureLock© Precast Gel System (Novex). Protein was the transferred to nitrocellulose membrane and blocked with 5% BSA in TBST or 5% Skimmed Milk in TBST dependent on the antibody (see table below). Primary antibodies were incubated at 4 °C overnight, blots were washed in TBST and secondary antibody was added at 1:5000 for 1 hour at room temperature. The blots were then washed again before application of Western Lightning© Plus ECL chemiluminescence for 1 minute. The blot was then exposed to X-ray film (Biomax MR Film, Kodak) developed using a JP-33 Film Processor (JPI Healthcare) and subsequently scanned on an HP flat-bed scanner.

Antibodies used in western blotting.

Antibody	Concentration
Goat α h/m polyclonal LPL (R&D Systems)	1:1000 (5% BSA/TBST)

Mouse α CD36 (FA6-152) (Abcam)	1:2000 (5% BSA/TBST)
Rabbit α FASN (C20G5) (Cell Signalling)	1:1000 (5% BSA/TBST)
Rabbit α ERK2 (Santa Cruz)	1:2000 (5% Milk/TBST)
Rabbit α β-Tubulin (Santa Cruz)	1:2000 (5% Milk/TBST)
HRP conjugated Donkey α Goat Secondary (Santa Cruz)	1:5000 (5% Milk/TBST)
HRP conjugated Donkey α Rabbit Secondary (GE Healthcare)	1:5000 (Mirrors Primary)
HRP conjugated Sheep α Mouse Secondary (GE Healthcare)	1:5000 (Mirrors Primary)

Immunohistochemistry for LPL

4μm sections obtained from formalin-fixed, paraffin-embedded archive samples, were stained by immunochemistry. Briefly, after deparaffinisation, antigen retrieval was performed by heating the slides placed in a TRIS-Buffer pH 9 using a pressure cooker. A mouse monoclonal antibody A4 against human LPL (ab21356, Abcam) diluted 1:300 was then applied for 120 minutes at room temperature. Secondary staining was performed using the Dako REAL detection System, Alkaline Phosphatase/RED, Rabbit/Mouse kit, based on the labelled streptavidin-biotin method. The diagnosis as well as the intensity of staining and the proportion of positive tumor cells were ascertained for each sample by a clinical dermatopathologist (JK).

Results

Transcriptome analysis reveals deregulated lipid metabolic pathways in advanced melanocyte neoplasia

Previously, we generated transgenic zebrafish displaying different grades of melanocyte neoplasia. Transgenic animals expressing $BRAF^{V600E}$ alone develop benign melanocyte hyperplasia, manifested as broader and darker stripes, while expression of $HRAS^{G12V}$ alone results in malignant melanocyte neoplasia that initially expands horizontally in the epidermis and hypodermis enveloping the entire body other than the ventral surface (the radial growth phase or RGP), and then vertically, infiltrating the subcutaneous tissue (the vertical growth phase or VGP) and resulting in mainly raised tumour nodules (Fig. 1A) (15). To minimize contamination from mRNA arising from non-diseased tissue that could add noise and drown out signal, transcriptome profiling was performed on RNA extracted from caudal fins of wild-type, $BRAF^{V600E}$ or $HRAS^{G12V}$ transgenic animals or tumour nodules located within caudal fins of $HRAS^{G12V}$ transgenic animals, using a customised Agilent 44K zebrafish transcriptome microarray (26).

Considering only genes with highly significant (P<0.0001) differential expression to minimise false positives and a fold-change of at least 2 compared to wild-type (Supp. Table 1), the VGP tumour model had the greatest number of differentially expressed genes (DEGs) totalling 4,429 (Fig. 1B). Hierarchical clustering of DEGs suggested a closer relationship between RGP and VGP profiles than any other two-way comparison (Fig. 1C). Indeed, a sizeable proportion of DEGs were shared in common between RGP and VGP demonstrating potentially step-wise progression, but much less so between BRAF and RAS models reflecting their very different progression pathways (Fig. 1D). Several groups have shown that melanoma develops independently from benign neoplasia and this extends to gene expression programs (35). Further, melanocytes expressing $BRAF^{V600E}$ alone have likely undergone a course of proliferation and senescence (25) that would mean samples are divergent both from wild type skin as well as from the V12RAS model. Many unique DEGs were detected in V12RAS-driven VGP melanocyte neoplasia. This is to be expected as melanomas increase their genetic diversity as they progress, while hypoxia in larger lesions also generates significant changes in gene transcription (36).

DEGs were converted to human orthologues using BioBDnet and BioMart, which were then subjected to Gene Ontology (GO) enrichment analysis for biological processes. GO enrichment analysis of the VGP up-regulated genes highlighted metabolism as an altered process, relating to 19% of up-regulated genes of which lipid metabolism genes constituted 28% (Fig. 1E; see also Supp. Table 2 for a list of genes comprising this ontology that are also exclusive to the VGP samples). Over-represented GO terms associated with RGP up-regulated genes included cell communication, signal transduction, developmental process and MAPK signalling cascade, while development and signal transduction related GO terms were enriched for BRAF up-regulated genes. In contrast to VGP, lipid metabolism GO terms were not significantly over-represented in up-regulated genes in RGP or VBRAF models (Supp Fig. 1).

Melanocyte tumours scavenge exogenous free fatty acids

Two gene products, LPL and FABP7, encoded by the VGP DEGs *lpl* (up-regulated 9.5-fold exclusively in VGP) and *fabp7a* (up-regulated 24.5-fold), are implicated in fatty acid scavenging in cancer (23). We also detected 40.5-fold up-regulation of the fatty acid transporter FATP2/SLC27A2 in VGP samples, which encodes a long-chain fatty acid transporter highly related to FATP1/SLC27A1, recently described as being enriched in melanoma compared to other cancer types and linked to melanoma development (9). LPL secreted by cells into the interstitial space and presented on the vasculature glycocalyx hydrolyses dietary triglycerides transported as chylomicrons or very low density lipoprotein to release free fatty acids, which can then be transported across the plasma membrane by fatty acid transporters such as CD36, FABP7, FATP1 and FATP2.

LPL and FABP7 are overexpressed in several cancers (23, 37). Increased expression of FABP7 has been observed in human melanoma, and expression correlates with aggressive tumours and poor prognosis (10-12). These findings suggest melanoma tumours increase their fatty acid scavenging in order to deal with an increased demand for fatty acids.

In order to image free fatty acid uptake by tissues *in vivo*, we employed [^{18}F]-FTHA, a radiolabelled palmitic acid analogue, as a PET tracer (21). A PET imaging protocol was developed for zebrafish (see methods) that did not require modification to the PET scanner. PET scans of wild-type fish 2 hours post administration revealed [^{18}F]-FTHA accumulation predominantly in the anterior abdomen (Fig. 2A). However, due to the limited spatial resolution, it was difficult from the PET scans alone to specify where [^{18}F]-FTHA had been taken up. Therefore, DESI-MS imaging was carried out after PET scans, in order to utilise its high spatial resolution to determine a more precise location for the tracer. The concentration of FTHA used for PET (~8 nmol/L) was, however, below the limit of detection of DESI-MS. Therefore, unlabelled FTHA was added at a higher concentration. DESI-MS imaging of wild-type fish with higher FTHA dosing (8 µmol/L) revealed that FTHA accumulated mainly in the liver (Fig. 2B), where dietary fatty acids are converted into triglycerides for incorporation into lipoproteins for distribution around the body. DESI-MS/MS was then carried out on sections in order to confirm that the negative ion mode peak at m/z 305.30 was indeed FTHA, and not an endogenous species. This yielded a diagnostic ion with m/z 205.18 (Supp Fig. 2). Previous studies have shown that although FTHA will predominantly enter the β-oxidation pathway, it can also be incorporated into phospholipids via lipogenesis with the pathway it is used by being tissue dependent (38). DESI-MS/MS was performed for lipid peaks co-localising with FTHA in the liver. One of these peaks (m/z 861) yielded small amounts of FTHA that had been incorporated into this lipid after 30 mins exposure (Supp Fig. 3). However, identification of m/z 861 was not possible, as spectra were indicative of more than one unresolved lipid at m/z 861. Nevertheless, this finding indicates that FTHA can enter the lipogenesis pathway, at least in liver cells.

Next, PET scans of V12RAS transgenic zebrafish bearing tumour nodules revealed concentration of [^{18}F]-FTHA in 8/8 tumours (Fig. 2C and D), consistent with fatty acid uptake being elevated in V12RAS-transformed melanocytes as predicted from transcriptomics. Previously it was shown that enhanced fatty acid uptake through increased expression of FATP1 in zebrafish melanoma cells resulted in increased fatty acid storage as lipid droplets, while FATP1 expression was shown to correlate with lipid droplets in patient melanoma biopsies (9). Using Nile Red staining we detected abundant lipid droplets in V12RAS-driven melanoma nodules, again consistent with increased fatty acid uptake (Supp Fig. 4A,B). As in wild-type animals, FTHA was not detected by DESI-MS in the tumour-bearing fish using the concentrations used in PET. Therefore,

fish were treated with a higher concentration of unlabelled FTHA (8 µmol/L) prior to DESI-MS imaging. In the representative example shown, FTHA localised in both snout and tail tumours as well as in the liver (Fig. 2E-H). Whereas uptake of FTHA was homogenous in the snout tumour, uptake was heterogeneous in the fin tumour (a finding that would not be apparent by PET scans alone) and did not co-localise with areas of the most densely packed cells, as may have been expected. Both PET and DESI-MS indicated that FTHA accumulation was markedly higher in tumour nodules than flat areas of skin containing only RGP melanoma, consistent with our transcriptomic analysis identifying up-regulation of fatty acid scavenging genes selectively in VGP melanoma.

Glycerophospholipid metabolism is deregulated in malignant melanocyte neoplasia

UHPLC-MS metabolomics was performed on non-aqueous solvent extracts of wild-type skin, skin containing RGP melanoma, and on VGP tumour nodules excised from the body wall to determine changes in metabolite concentration during melanocyte neoplasia progression. A number of species from all lipid metabolite classes changed in abundance compared to wild-type skin, increasing with disease progression and mirroring the diversity seen in the transcriptome (see Supp. Table 3 and Supp Fig. 5A,B). PCA of metabolites detected by UHPLC-MS indicated a clear separation between wild-type, RGP and VGP samples with a more significant separation observed for negative ion mode data (Fig. 3A). The transcriptome and metabolome data were integrated using MetScape, which highlighted the glycerophospholipid metabolism pathway in both the VGP (Fig. 3B) and RGP (Supp. Fig. 5C) samples. Major components of the cell membrane include phosphatidyl choline (PC) and phosphatidyl ethanolamine (PE) species, which increased in relative abundance in zebrafish V12RAS-driven melanocyte neoplasia, beginning in the RGP model and becoming more prominent in the VGP model. This change was also accompanied by a depletion of phosphatidylserine (PS), potentially driven by increased expression of phosphatidylserine decarboxylase (PISD), as revealed by the transcriptome analysis (up-regulated 3.7-fold exclusively in VGP), which catalyzes the formation of PE by decarboxylation of PS. DESI-MS was carried out to visualise phospholipid species in VGP melanoma tumours. As well as revealing clear differences in glycerophospholipid abundance between the tumour and healthy tissue, imaging revealed heterogeneity of glycerophospholipid species, including PE species in the tumour (Fig. 3 C,D and Supp Fig. 6A,B).

LPL is a potential therapeutic target especially when de novo fatty acid synthesis is not enhanced by FASN up-regulation

To evaluate the potential for fatty acid scavenging in human melanoma, we quantified expression of *LPL*, *CD36*, *FABP7*, *FATP1* and *FATP2* mRNA by reverse-transcription coupled real-time PCR (RT-PCR) in a panel of established human melanoma cell lines (Supp. Table 4) and contrasted this to levels in normal human melanocytes (NHM). This revealed elevated *LPL* transcript in all the melanoma cell lines, both NRAS and BRAF mutant, across a wide range of fold-changes compared to NHM (Fig 4A). Elevation of *LPL* mRNA reached more than 40-fold, whereas fewer instances of significant mRNA upregulation for the fatty acid transporters were observed, and fold-change was only ever modest (less than 5-fold). Western blotting for LPL on protein lysates extracted from melanoma cell lines in this panel revealed elevated protein compared to melanocytes consistent with the extent of mRNA upregulation (Supp. Fig. 7A), increased LPL expression was also confirmed by immunofluorescence staining for LPL (Supp. Fig. 7B). Moreover, positive immunohistochemistry staining revealed LPL expression in 90% or more of primary and metastatic melanoma tumours (Fig. 4B). LPL was also detected in 77% of naevi, but was largely restricted to nests of naevocytes occupying the junction between the epidermis and the dermis (Fig. 4C). LPL staining appeared specific, as outside the tumour a positive signal was detected, as expected (39), only in adipocytes and capillary lumens (Supp. Fig. 7C). There were significantly more examples of strong LPL staining (++ and +++) in melanoma cases (primary and metastatic) compared to naevi ($p = 0.005$, χ^2 test).

By investigating mRNA expression for LPL and the fatty acid transporters listed above in cutaneous melanoma cases collected and analysed by the Cancer Genome Atlas network (40), we found no significant effect from NRAS and BRAF mutation status (Supp. Fig. 8A). LPL mRNA expression was most highly correlated with CD36 mRNA followed by FABP7 mRNA, and there was no correlation between LPL expression and either FATP1 or FATP2 mRNA expression (Supp. Fig. 8B). Further, although fatty acid scavenging was shown to enhance metastasis of melanoma cells (13), mRNA for LPL and the fatty acid transporters listed above was not more abundant in metastatic samples in the TCGA collection than primary lesions (Supp. Fig. 8C), and there was no difference evident in LPL expression in metastases vs primary from immunohistochemistry (Fig. 4B; $p = 0.91$, χ^2 test). Therefore enhanced fatty acid scavenging is most likely a common feature of both primary and secondary tumours.

Upregulation of LPL mRNA was only detected in VGP zebrafish melanocyte neoplasia (not in RGP or benign neoplasia models). To determine whether in this V12RAS driven-model upregulation of LPL is sufficient to enhance progression from RGP to VGP, we turned to a transient transgenesis assay originally devised to detect co-operation between oncogenic BRAF and other candidate melanoma oncogenes (25). The V12RAS transgene was crossed into a *mitfa* mutant background to suppress melanocyte development. One-cell stage eggs from these animals were then injected with a plasmid containing a wild-type *mitfa* minigene to rescue

melanocyte development while expressing a second *mitfa*-promoter driven cassette encoding either mCherry (as a negative control), LPL or CCND1 (a positive control) (Supp. Fig. 9A,B). Tumour nodule formation was then followed in animals where pigmentation had been nearly completely restored while embryos. All pigment-rescued animals developed the characteristic RGP appearance of the parent V12RAS line (Fig. 5A). Compared to mCherry, however, co-expression of LPL accelerated tumour nodule formation comparable to CCND1 (Fig. 5B). Moreover, co-expression of LPL increased tumour growth rate compared to either mCherry or CCND1 (Fig. 5C). Using the same transient transgenesis approach, a weaker but still significant cooperation was also observed with NRASG12D (Supp. Fig. 9C,D).

Turning to human melanoma cells, knockdown of LPL using two independent siRNA oligonucleotides reduced cell growth by as much as 70% in WM852 cells and 50% in WM266-4 cells, but did not affect A375 cells (Fig. 5D). To address the difference in sensitivity to suppressing LPL in melanoma cells we evaluated expression of FASN required for *de novo* fatty acid synthesis by reverse transcription coupled RT-PCR and western blotting. FASN mRNA and protein levels were significantly higher in A375 cells and WM266-4 cells relative to primary melanocytes but also compared to WM852 cells (Fig. 5E and Supp Fig. 9E), implying *de novo* fatty acid synthesis may complement fatty acid scavenging in A375 and WM266-4 cells but not WM852 cells. WM852 cells were also more sensitive to a small molecule inhibitor of LPL (GSK264220A) (41) than either A375 cells or WM266-4 cells (Fig. 5F). Significantly, combined treatment with FASN inhibitor C75 (42) and LPL inhibitor synergized to suppress the growth of A375 cells and WM266-4 cells but not WM852 cells (Fig. 5F). Moreover, FASN expression is relatively low in WM1361 cells and high in WM35 cells (Fig. 5E and Supp Fig. 9E) and consistent with predictions from above WM1361 cells were sensitive to LPL inhibitor with no added effect of FASN inhibitor, while WM35 were less sensitive to LPL inhibitor but could be sensitized by addition of FASN inhibitor (Fig. 5F).

Discussion

Fatty acids are used by cells for both energy production (β-oxidation) and lipogenesis to form membrane phospholipids. As cancer cells have higher energy demands and proliferate at higher rates than healthy cells, increased acquisition of fatty acids can be expected. However, tumours can acquire fatty acids by different mechanisms: uptake from outside the cell or *de novo* synthesis (5). VGP up-regulated DEGs included *lpl, fabp7a*, and *fatp2*/*slc27a2*, whose gene products are implicated in the uptake of exogenous fatty acid. Kamphorst *et al*. have shown that oncogenic RAS-driven tumours source fatty acids by scavenging them as lysophospholipids (43), demonstrating also that RAS-driven tumours are dependent on fatty acid scavenging. It has also recently been reported that the up-regulation of the scavenger fatty acid receptor, CD36, is

correlated to metastases and poor prognosis in melanoma and is a marker of tumour initiating cells (13). Of interest, culturing melanoma cells with adipocytes stimulates melanoma cell proliferation and this affect could be reproduced with palmitate alone. Further, the transfer of fatty acid from adipocytes to melanoma cells could be directly visualised (8). Indeed, proximity to adipose has been demonstrated to facilitate the development of zebrafish melanocyte neoplasia through the supply of exogenous fatty acid and this could be inhibited using a FATP inhibitor (9). It is notable that relative to normal skin we observed reduced triglyceride levels in both RGP and VGP V12RAS-driven melanocyte neoplasia, in keeping with depletion of adipose lipid reserves.

Tumour cells can also synthesise fatty acids *de novo*, and FASN and SCD-1 are crucial enzymes in this pathway. FASN synthesises palmitate from acetyl-CoA and malonyl-CoA, and palmitate can undergo subsequent changes such as elongation and desaturation. SCD-1 generates unsaturated fatty acids such as oleic acid (18:1) and palmitoleic acid (16:1), by inserting a double bond into a saturated fatty acid at the Δ9 position. FASN and SCD-1 have been found to be overexpressed in many cancers including melanoma (3, 4, 44), implying that *de novo* fatty acid production is also increased. *Scda* (6.5-fold) and *-b* (4.1-fold) overexpression but not *fasn* overexpression was also observed in zebrafish V12RAS-driven VGP melanocyte neoplasia. Since SCD1 could just as well desaturate fatty acids that are scavenged as synthesized *de novo*, its upregulation here does not necessarily indicate increased *de novo* synthesis. Cells can also break down phospholipids to generate free fatty acids. Expression of several PLA2 isoforms (*pla2g6*, *pla2g7* and *pla2g10*) appeared to be up-regulated (2.0-5.3 fold) in zebrafish V12RAS-driven VGP melanocyte neoplasia. PLA2 enzymes are a diverse family of phospholipases which hydrolyse phospholipids to generate free fatty acids (commonly arachidonic acid) and lysophospholipids. Lysophospholipids and arachidonic acid are both signalling molecules, with arachidonic acid being a precursor of several bioactive eicosanoids, which in turn are involved in inflammatory mechanisms. PLA2 deregulation in cancer is increasingly recognised (45) with the PLA2G6 gene being associated with heightened risk of malignancy developing in naevi (46, 47), and the PLA2 family being investigated as a source of potential drug targets (45).

PET and DESI-MS imaging using the palmitic acid analogue FTHA were used as complementary imaging modalities to reveal enhanced fatty acid scavenging in zebrafish melanocyte neoplasia, implied by the transcriptomic data. Melanocyte tumours may be scavenging palmitate (and hence FTHA) to be used in β-oxidation or in lipogenesis. β-oxidation provides an alternative energy source to glucose and has been linked with the metastatic phenotype of melanoma cell lines (48). Lipogenesis rates will also be increased in cancer, and so it is plausible that FTHA may also be incorporated into more complex lipids. Indeed, a previous study found that exogenous palmitate was incorporated into glycerophospholipids, sphingolipids, and ether lipids

in a range of human cancer cells (49). However, no lipids were found that co-localised exactly with the FTHA distribution in tumours, making targeted MS/MS experiments difficult. It is possible that administering the FTHA for a longer period of time would give rise to more lipids containing FTHA as a fatty acid chain.

In order to understand changes to lipid metabolism more precisely, transcriptome data were integrated with UHPLC-MS metabolome data. This integrated approach, further corroborated by DESI-MS imaging, highlighted the glycerophospholipid metabolism pathway, which is critical to the synthesis of plasma membrane phospholipids, playing a role in melanocyte neoplasia progression. Aberrant glycerophospholipid metabolism has previously been implicated in melanoma metastatic potential (50). Phospholipids, including PC and PE species, were up-regulated in VGP tumours compared to the surrounding healthy tissue, while PS species were down-regulated. Of note, the mitochondrial protease Lactamase Beta (LACTB) has been shown to exert its tumour suppressor function through regulating the stability of PISD, which we observed to be up-regulated in zebrafish V12RAS-driven melanocyte VGP neoplasia. Loss of LACTB expression in oncogene-expressing breast epithelial cells resulted in elevation of PISD protein accompanied by a conversion of mitochondrial PS to PE and lysoPE that was necessary for cancer cell proliferation and dedifferentiation (51). Additionally, lipidomics comparing lipid species in human and zebrafish BRAF mutant melanoma cells co-cultured with adipocytes to those cultured alone, or those recovered from tumors *in vivo* contrasted to those cultured *in vitro* also revealed increased PC and PE species (9), indicating that our V12RAS-driven zebrafish melanocyte malignancies resemble oncogenic BRAF-driven malignant melanocytes stimulated by adipocytes. Choline containing biomolecules are increased in human primary and metastatic melanoma when measured by magnetic resonance imaging (52, 53) as in other cancers such as prostate cancer (54). Indeed, altered anabolism but also catabolism of PC (to produce important signalling molecules such as diacylglyceride) are now considered a pervasive feature of cancer cell metabolism and intracellular signalling (55). Phospholipase D1, up-regulated (2.1-fold) in zebrafish V12RAS-driven VGP melanocyte neoplasia, which removes the choline head group, is essential for $HRAS^{G12V}$-mediated transformation and tumour formation (56) and is up-regulated also in human melanoma (57). Thus choline metabolism too emerges as a potential target for therapeutic intervention in melanoma.

Although both the DESI-MS and UHPLC-MS use electrospray as the ionisation source, different solvents were used for each experiment therefore giving rise to different adducts. In this respect, both similar and different lipid species were expected to be detected between the two techniques. Fig. 3C shows DESI-MS images of two of the species also seen up-regulated in tumours in the UHPLC-MS analysis (m/z 714.52 and 776.54) as well as two PEs that were not detected by UHPLC-MS. The identified species both contain a monounsaturated fatty acid, indicating the action of SCD-1, which was revealed to be overexpressed in the

transcriptome analysis. UHPLC-MS is able to give a more quantitative analysis compared to DESI-MS, but UHPLC-MS cannot give information regarding spatial distribution. Interestingly, DESI-MS imaging revealed heterogeneous distributions of phospholipid species in VGP tumours. Positive ion mode images revealed lipids with interesting heterogeneity, and are potential PCs, based on database searches using accurate mass. However, identification of these lipids is not trivial due to multiple ionisation mechanisms (i.e. the addition of a proton, sodium or potassium), and therefore have not been identified in this instance. It is clear from this study that lipid metabolism is not a uniform process across the whole tumour, and further studies will be needed to elucidate the reasons behind such complexity in melanoma metabolism.

RT-PCR, western blotting and immunohistochemistry revealed LPL expression in a majority of melanoma samples, albeit to varying amounts and with varying fractions of positive cells. We hypothesize that at one extreme (represented in culture by WM852 and WM1361 cells and potentially in vivo by tumours with homogeneous strong LPL expression), melanoma cells depend entirely on LPL for fatty acid supply; while at the other end of the spectrum tumour cells are largely independent of LPL for fatty acid provision and may even not express LPL (a few primary tumours were identified seemingly lacking LPL expression). These latter cells (or even whole tumours) may rely entirely on *de novo* synthesis, or may express alternative lipases to carry out lipolysis. In between are cell populations (represented in culture by WM266-4, WM-35 and A375 cells) that express LPL for lipolysis and also undertake fatty acid synthesis, either representing a heterogeneous mixture of cell types, or with cells possessing both capabilities simultaneously. Coincident lipolysis and fatty acid synthesis has previously been described in breast carcinoma, liposarcoma and prostate carcinoma cells (58). Proximity to adipose and the availability of exogenous fatty acid has been shown to decrease dependency on lipogenesis in melanoma cells, concomitant with decreased sensitivity to FASN inhibition (9). Given the capacity of melanoma cells (and other cancer cells) to profit from both lipolytic and lipogenic mechanisms, it is desirable to explore strategies to target simultaneously both fatty acid scavenging and *de novo* synthesis. We demonstrated here the potential of an LPL small molecule inhibitor in combination with FASN inhibitor; lipid transporters such as FATP family members, FABP7 and CD36 might also make for appropriate targets.

In conclusion, zebrafish V12RAS-driven melanocyte tumours were seen to undergo substantial changes to their lipid metabolism. Multi-modality imaging combined with lipidome and transcriptome analyses has shown that zebrafish V12RAS-driven melanocyte tumours scavenge free fatty acids and upregulate the production of certain glycerophospholipids. Key lipid metabolism pathways are well-conserved between zebrafish and human and several overlaps between altered lipid metabolism genes in the zebrafish melanocyte neoplasia models studied here and human melanoma have been highlighted, supporting the

preclinical significance of our zebrafish models. This study demonstrated the complementarity of PET and DESI-MS as *in vivo* and *ex vivo* imaging modalities respectively that differ in spatial resolution as well as their targeted nature. Potentially, detection of fatty acid uptake by PET might be used to locate tumours in patients, as well as to stratify patients for treatment with inhibitors of fatty acid scavenging, or to monitor therapeutic intervention. The feasibility of [^{18}F]-FTHA PET in humans has already been demonstrated (59), albeit not yet for tumour imaging. UHPLC-MS and DESI-MS could be used on biopsy samples, and so also have the potential to inform treatments in the clinic. Combining lipidomics and transcriptomics reveals a more complete picture of altered tumour lipid metabolism than either alone. While deregulated lipid metabolism pathways are promising targets for future therapeutic intervention, the heterogeneous nature in which lipid metabolism is altered must also be taken into consideration and combinatorial approaches are likely to be more effective than monotherapies.

Acknowledgements

Work presented here was supported by the European Research Council grant ERC-2011-StG-282059 PROMINENT to AH and by the Cancer Research UK (CRUK) and Engineering and Physical Sciences Research Council (EPSRC) Manchester and Cambridge Cancer Imaging Centre grant C8742/A18097 to KW and AM. HJ was funded by a BBSRC PhD studentship and Christie Charity award. We would like to thank Paul Begley for his technical support.

References

1. Beloribi-Djefaflia S, Vasseur S, Guillaumond F. Lipid metabolic reprogramming in cancer cells. Oncogenesis. 2016;5:e189.
2. Gniadecka M, Philipsen PA, Sigurdsson S, Wessel S, Nielsen OF, Christensen DH, et al. Melanoma diagnosis by Raman spectroscopy and neural networks: structure alterations in proteins and lipids in intact cancer tissue. The Journal of investigative dermatology. 2004;122:443-9.
3. Innocenzi D, Alo PL, Balzani A, Sebastiani V, Silipo V, La Torre G, et al. Fatty acid synthase expression in melanoma. J Cutan Pathol. 2003;30:23-8.
4. Kapur P, Rakheja D, Roy LC, Hoang MP. Fatty acid synthase expression in cutaneous melanocytic neoplasms. Mod Pathol. 2005;18:1107-12.
5. Rohrig F, Schulze A. The multifaceted roles of fatty acid synthesis in cancer. Nat Rev Cancer. 2016;16:732-49.
6. Carvalho MA, Zecchin KG, Seguin F, Bastos DC, Agostini M, Rangel AL, et al. Fatty acid synthase inhibition with Orlistat promotes apoptosis and reduces cell growth and lymph node metastasis in a mouse melanoma model. Int J Cancer. 2008;123:2557-65.
7. Zecchin KG, Rossato FA, Raposo HF, Melo DR, Alberici LC, Oliveira HC, et al. Inhibition of fatty acid synthase in melanoma cells activates the intrinsic pathway of apoptosis. Lab Invest. 2011;91:232-40.
8. Kwan HY, Fu X, Liu B, Chao X, Chan CL, Cao H, et al. Subcutaneous adipocytes promote melanoma cell growth by activating the Akt signaling pathway: role of palmitic acid. J Biol Chem. 2014;289:30525-37.
9. Zhang M, Martino JSD, Bowman RL, Campbell NR, Baksh SC, Simon-Vermot T, et al. Adipocyte-Derived Lipids Mediate Melanoma Progression via FATP Proteins. Cancer discovery. 2018.
10. Goto Y, Koyanagi K, Narita N, Kawakami Y, Takata M, Uchiyama A, et al. Aberrant fatty acid-binding protein-7 gene expression in cutaneous malignant melanoma. The Journal of investigative dermatology. 2010;130:221-9.
11. Slipicevic A, Jørgensen K, Skrede M, Rosnes AK, Trøen G, Davidson B, et al. The fatty acid binding protein 7 (FABP7) is involved in proliferation and invasion of melanoma cells. BMC Cancer. 2008;8:276.
12. Goto Y, Matsuzaki Y, Kurihara S, Shimizu A, Okada T, Yamamoto K, et al. A new melanoma antigen fatty acid-binding protein 7, involved in proliferation and invasion, is a potential target for immunotherapy and molecular target therapy. Cancer Res. 2006;66:4443-9.
13. Pascual G, Avgustinova A, Mejetta S, Martin M, Castellanos A, Attolini CS, et al. Targeting metastasis-initiating cells through the fatty acid receptor CD36. Nature. 2017;541:41-5.
14. van der Weyden L, Patton EE, Wood GA, Foote AK, Brenn T, Arends MJ, et al. Cross-species models of human melanoma. J Pathol. 2016;238:152-65.

15. Michailidou C, Jones M, Walker P, Kamarashev J, Kelly A, Hurlstone AF. Dissecting the roles of Raf- and PI3K-signalling pathways in melanoma formation and progression in a zebrafish model. Dis Model Mech. 2009;2:399-411.
16. Dalton LE, Kamarashev J, Barinaga-Rementeria Ramirez I, White G, Malliri A, Hurlstone A. Constitutive RAC activation is not sufficient to initiate melanocyte neoplasia but accelerates malignant progression. The Journal of investigative dermatology. 2013;133:1572-81.
17. Hara T, Inagaki K, Kosaka N, Morita T. Sensitive detection of mediastinal lymph node metastasis of lung cancer with 11C-choline PET. J Nucl Med. 2000;41:1507-13.
18. Hara T, Kosaka N, Kishi H. PET imaging of prostate cancer using carbon-11-choline. J Nucl Med. 1998;39:990-5.
19. Oyama N, Akino H, Kanamaru H, Suzuki Y, Muramoto S, Yonekura Y, et al. 11C-acetate PET imaging of prostate cancer. J Nucl Med. 2002;43:181-6.
20. Tsuchida T, Takeuchi H, Okazawa H, Tsujikawa T, Fujibayashi Y. Grading of brain glioma with 1-11C-acetate PET: comparison with 18F-FDG PET. Nucl Med Biol. 2008;35:171-6.
21. DeGrado TR, Wang S, Holden JE, Nickles RJ, Taylor M, Stone CK. Synthesis and preliminary evaluation of (18)F-labeled 4-thia palmitate as a PET tracer of myocardial fatty acid oxidation. Nucl Med Biol. 2000;27:221-31.
22. Takats Z, Wiseman JM, Gologan B, Cooks RG. Mass spectrometry sampling under ambient conditions with desorption electrospray ionization. Science. 2004;306:471-3.
23. Balaban S, Lee LS, Schreuder M, Hoy AJ. Obesity and Cancer Progression: Is There a Role of Fatty Acid Metabolism? BioMed Research International. 2015;2015:17.
24. Casar B, Badrock AP, Jimenez I, Arozarena I, Colon-Bolea P, Lorenzo-Martin LF, et al. RAS at the Golgi antagonizes malignant transformation through PTPRkappa-mediated inhibition of ERK activation. Nature communications. 2018;9:3595.
25. Ceol CJ, Houvras Y, Jane-Valbuena J, Bilodeau S, Orlando DA, Battisti V, et al. The histone methyltransferase SETDB1 is recurrently amplified in melanoma and accelerates its onset. Nature. 2011;471:513-7.
26. Stockhammer OW, Zakrzewska A, Hegedus Z, Spaink HP, Meijer AH. Transcriptome profiling and functional analyses of the zebrafish embryonic innate immune response to Salmonella infection. J Immunol. 2009;182:5641-53.
27. Mudunuri U, Che A, Yi M, Stephens RM. bioDBnet: the biological database network. Bioinformatics. 2009;25:555-6.
28. Kinsella RJ, Kähäri A, Haider S, Zamora J, Proctor G, Spudich G, et al. Ensembl BioMarts: a hub for data retrieval across taxonomic space. Database. 2011;2011:bar030-bar.

29. The Gene Ontology Consortium. Expansion of the Gene Ontology knowledgebase and resources. Nucleic Acids Research. 2017;45:D331-D8.
30. Degrado TR. Synthesis of 14(R,S)-[F-18]Fluoro-6-Thia-Heptadecanoic Acid (Ftha). Journal of Labelled Compounds & Radiopharmaceuticals. 1991;29:989-95.
31. Sud M, Fahy E, Cotter D, Brown A, Dennis EA, Glass CK, et al. LMSD: LIPID MAPS structure database. Nucleic Acids Research. 2007;35:D527-D32.
32. Brown M, Wedge DC, Goodacre R, Kell DB, Baker PN, Kenny LC, et al. Automated workflows for accurate mass-based putative metabolite identification in LC/MS-derived metabolomic datasets. Bioinformatics. 2011;27:1108-12.
33. Sumner LW, Amberg A, Barrett D, Beale MH, Beger R, Daykin CA, et al. Proposed minimum reporting standards for chemical analysis Chemical Analysis Working Group (CAWG) Metabolomics Standards Initiative (MSI). Metabolomics. 2007;3:211-21.
34. Karnovsky A, Weymouth T, Hull T, Tarcea VG, Scardoni G, Laudanna C, et al. Metscape 2 Bioinformatics Tool for the Analysis and Visualization of Metabolomics and Gene Expression Data. Bioinformatics. 2011.
35. Rose AE, Poliseno L, Wang J, Clark M, Pearlman A, Wang G, et al. Integrative genomics identifies molecular alterations that challenge the linear model of melanoma progression. Cancer Res. 2011;71:2561-71.
36. Chi JT, Wang Z, Nuyten DS, Rodriguez EH, Schaner ME, Salim A, et al. Gene expression programs in response to hypoxia: cell type specificity and prognostic significance in human cancers. PLoS Med. 2006;3:e47.
37. Zaidi N, Lupien L, Kuemmerle NB, Kinlaw WB, Swinnen JV, Smans K. Lipogenesis and lipolysis: the pathways exploited by the cancer cells to acquire fatty acids. Prog Lipid Res. 2013;52:585-9.
38. Takala TO, Nuutila P, Pulkki K, Oikonen V, Gronroos T, Savunen T, et al. 14(R,S)-[18F]Fluoro-6-thia-heptadecanoic acid as a tracer of free fatty acid uptake and oxidation in myocardium and skeletal muscle. Eur J Nucl Med Mol Imaging. 2002;29:1617-22.
39. Davies BSJ, Beigneux AP, Barnes RH, Tu Y, Gin P, Weinstein MM, et al. GPIHBP1 Is Responsible for the Entry of Lipoprotein Lipase into Capillaries. Cell Metabolism. 2010;12:42-52.
40. Cancer Genome Atlas N. Genomic Classification of Cutaneous Melanoma. Cell. 2015;161:1681-96.
41. Keller PM, Rust T, Murphy DJ, Matico R, Trill JJ, Krawiec JA, et al. A high-throughput screen for endothelial lipase using HDL as substrate. J Biomol Screen. 2008;13:468-75.
42. Kuhajda FP, Pizer ES, Li JN, Mani NS, Frehywot GL, Townsend CA. Synthesis and antitumor activity of an inhibitor of fatty acid synthase. Proc Natl Acad Sci U S A. 2000;97:3450-4.

43. Kamphorst JJ, Cross JR, Fan J, de Stanchina E, Mathew R, White EP, et al. Hypoxic and Ras-transformed cells support growth by scavenging unsaturated fatty acids from lysophospholipids. Proc Natl Acad Sci U S A. 2013;110:8882-7.
44. von Roemeling CA, Marlow LA, Wei JJ, Cooper SJ, Caulfield TR, Wu K, et al. Stearoyl-CoA desaturase 1 is a novel molecular therapeutic target for clear cell renal cell carcinoma. Clin Cancer Res. 2013;19:2368-80.
45. Scott KF, Sajinovic M, Hein J, Nixdorf S, Galettis P, Liauw W, et al. Emerging roles for phospholipase A2 enzymes in cancer. Biochimie. 2010;92:601-10.
46. Bishop DT, Demenais F, Iles MM, Harland M, Taylor JC, Corda E, et al. Genome-wide association study identifies three loci associated with melanoma risk. Nature genetics. 2009;41:920-5.
47. Mario F, Veronique B, Nicholas HK, David DL, Julia NBA, Tomi P, et al. Loci at 9p21 and 22q13 harbour alleles for development of cutaneous nevi and melanoma. Nature genetics. 2009;41:915-9.
48. Rodrigues MF, Obre E, de Melo FH, Santos GC, Jr., Galina A, Jasiulionis MG, et al. Enhanced OXPHOS, glutaminolysis and beta-oxidation constitute the metastatic phenotype of melanoma cells. Biochem J. 2016;473:703-15.
49. Louie SM, Roberts LS, Mulvihill MM, Luo K, Nomura DK. Cancer Cells Incorporate and Remodel Exogenous Palmitate into Structural and Oncogenic Signaling Lipids. Biochimica et biophysica acta. 2013;1831:10.1016/j.bbalip.2013.07.008.
50. Kim HY, Lee H, Kim SH, Jin H, Bae J, Choi HK. Discovery of potential biomarkers in human melanoma cells with different metastatic potential by metabolic and lipidomic profiling. Scientific reports. 2017;7:8864.
51. Keckesova Z, Donaher JL, De Cock J, Freinkman E, Lingrell S, Bachovchin DA, et al. LACTB is a tumour suppressor that modulates lipid metabolism and cell state. Nature. 2017;543:681-6.
52. Guitera P, Bourgeat P, Stretch JR, Scolyer RA, Ourselin S, Lean C, et al. Diagnostic value of 8.5 T magnetic resonance spectroscopy of benign and malignant skin lesion biopsies. Melanoma Res. 2010;20:311-7.
53. Fedele TA, Galdos-Riveros AC, Jose de Farias e Melo H, Magalhães A, Maria DA. Prognostic relationship of metabolic profile obtained of melanoma B16F10. Biomed Pharmacother. 2013;67:146-56.
54. Giskeødegård GF, Hansen AF, Bertilsson H, Gonzalez SV, Kristiansen KA, Bruheim P, et al. Metabolic markers in blood can separate prostate cancer from benign prostatic hyperplasia. Br J Cancer. 2015;113:1712-9.
55. Glunde K, Bhujwalla ZM, Ronen SM. Choline metabolism in malignant transformation. Nat Rev Cancer. 2011;11:835-48.

56. Buchanan FG, McReynolds M, Couvillon A, Kam Y, Holla VR, Dubois RN, et al. Requirement of phospholipase D1 activity in H-RasV12-induced transformation. Proc Natl Acad Sci U S A. 2005;102:1638-42.
57. Oka M, Kageshita T, Ono T, Goto A, Kuroki T, Ichihashi M. Protein kinase C alpha associates with phospholipase D1 and enhances basal phospholipase D activity in a protein phosphorylation-independent manner in human melanoma cells. The Journal of investigative dermatology. 2003;121:69-76.
58. Kuemmerle NB, Rysman E, Lombardo PS, Flanagan AJ, Lipe BC, Wells WA, et al. Lipoprotein lipase links dietary fat to solid tumor cell proliferation. Mol Cancer Ther. 2011;10:427-36.
59. Iozzo P, Turpeinen AK, Takala T, Oikonen V, Solin O, Ferrannini E, et al. Liver uptake of free fatty acids in vivo in humans as determined with 14(R, S)-[18F]fluoro-6-thia-heptadecanoic acid and PET. Eur J Nucl Med Mol Imaging. 2003;30:1160-4.

Figure Legends

Fig.1: Transcriptome profiling identifies a gene signature associated with malignant progression. A) The four models from which fin or tumour samples were excised and RNA extracted. RGP, radial growth phase. VGP, vertical growth phase. **B)** Bar chart depicting the number of highly significant (P<0.0001, Kruskall Wallace test) differentially expressed genes (DEGs) with at least a two-fold difference in expression from wild-type in the different models. **C)** A heat map of gene expression following hierarchal clustering. **D)** Venn diagrams illustrating the extent of overlap in DEGs between the models**. E)** GO enrichment analysis reveals that 19% of DEGs in VGP samples are implicated in metabolism of which lipid metabolism genes represent 28%.

Fig. 2: PET and DESI-MS imaging of ([^{18}F])-FTHA in wild-type zebrafish and zebrafish bearing melanoma tumours. A) [^{18}F]-FTHA PET scans of wild-type zebrafish. **B)** (Upper panel) Negative ion mode DESI-MS image (120 µm spatial resolution) of FTHA distribution in a wild-type zebrafish, overlaid with an optical image. (Lower panel) An adjacent section was stained with H&E. C**)** [^{18}F]-FTHA PET scans of three tumour-bearing zebrafish. **D)** An optical image of one of the zebrafish that underwent PET scanning. **E)** DESI-MS image of FTHA distribution in the whole fish (50 µm resolution) **F)** DESI-MS image of FTHA distribution in the tail tumour (40 µm resolution). Images E and F have been overlaid with an ion appearing only in the skeletal muscle (m/z 154.1). **G)** and **H)** Corresponding H&E images. Arrows indicate tumours in the fish; this zebrafish has an obvious tumour in its tail, and a tumour in its snout which is apparent in the DESI-MS and H&E image.

Fig. 3: Altered glycerophospholipid metabolism accompanies melanocyte neoplasia progression. A) PCA analysis from UPLC-MS negative and positive ion modes demonstrates the significant difference between samples based on separation by principal component 1 and 2 (PC1 and PC2). QC refers to a pooled biological quality control sample run before and every fifth injection during analysis. **B)** Integration of lipid metabolite and lipid metabolism genes for tumour nodules (VGP) using Metscape reveals glycerophospholipid metabolism to be the most enriched network. Metabolites are indicated as hexagons and genes as circles. A darker colour demonstrates a greater degree of deregulation with the relative size of the symbol indicating up or down-regulation.
(See also http://ndexbio.org/#/network/e22027c9-6dbb-11e8-a4bf-0ac135e8bacf?accesskey=679ae449f48ae05d9116df1983f201390c539b285cc525ab149f2e178e55717e)**. C)** Negative ion mode DESI-MS images of the whole zebrafish, including an overlay with H&E stain where tumours have been circled (MS/MS spectra for m/z 720.50 and 734.53 species shown in Supp. Fig. 6A and B

respectively). **D)** Positive ion mode DESI-MS images of unidentified lipids in the tail tumour with corresponding H&E stain (left).

Fig. 4: LPL expression in human melanoma cell lines and tumours. A) Real-time PCR quantitation for LPL, CD36, FATP1, FATP2 and FABP7 mRNA expression in a panel of melanoma cell lines relative to normal human melanocytes (NHM). **B)** Positive immunohistochemical signal (pink/red) reveals LPL expression in a panel of naevi, primary tumours and metastases. -, absent staining; +, weak staining; ++, strong heterogeneous staining; +++, strong homogeneous staining. **C**) Representative image illustrating LPL expression (arrowheads) in nests of naevocytes at the epidermal/dermal junction in a compound naevus.

Fig. 5: LPL contributes to melanoma cell growth. A) A transgenic system for co-expression of LPL and V12RAS. *Upper panel* Uninjected V12RAS; *mitfa*$^{-/-}$ animal; *lower panel* V12RAS; *mitfa*$^{-/-}$ animal injected with *mitfa*-encoding plasmid displaying complete pigment rescue and a tumour nodule (arrow head). **B)** LPL co-expression accelerates tumour nodule appearance to the same extent as CCND1. ****, $p<0.0001$ Log-rank (Mantel-Cox) test. **C)** LPL co-expression accelerates tumour nodule growth **, $p<0.01$ Kruskal-Wallis test. **D)** Knockdown of LPL using siRNA suppresses cell growth. **, $p<0.01$; ***, $p<0.001$ ANOVA. **E)** Expression of FASN mRNA in a panel of melanoma cells relative to normal human melanocytes (NHM) detected by RT-PCR. **F)** Co-treatment of cells with GSK264220A (LPLi) and C75 (FASNi).

Figure 1

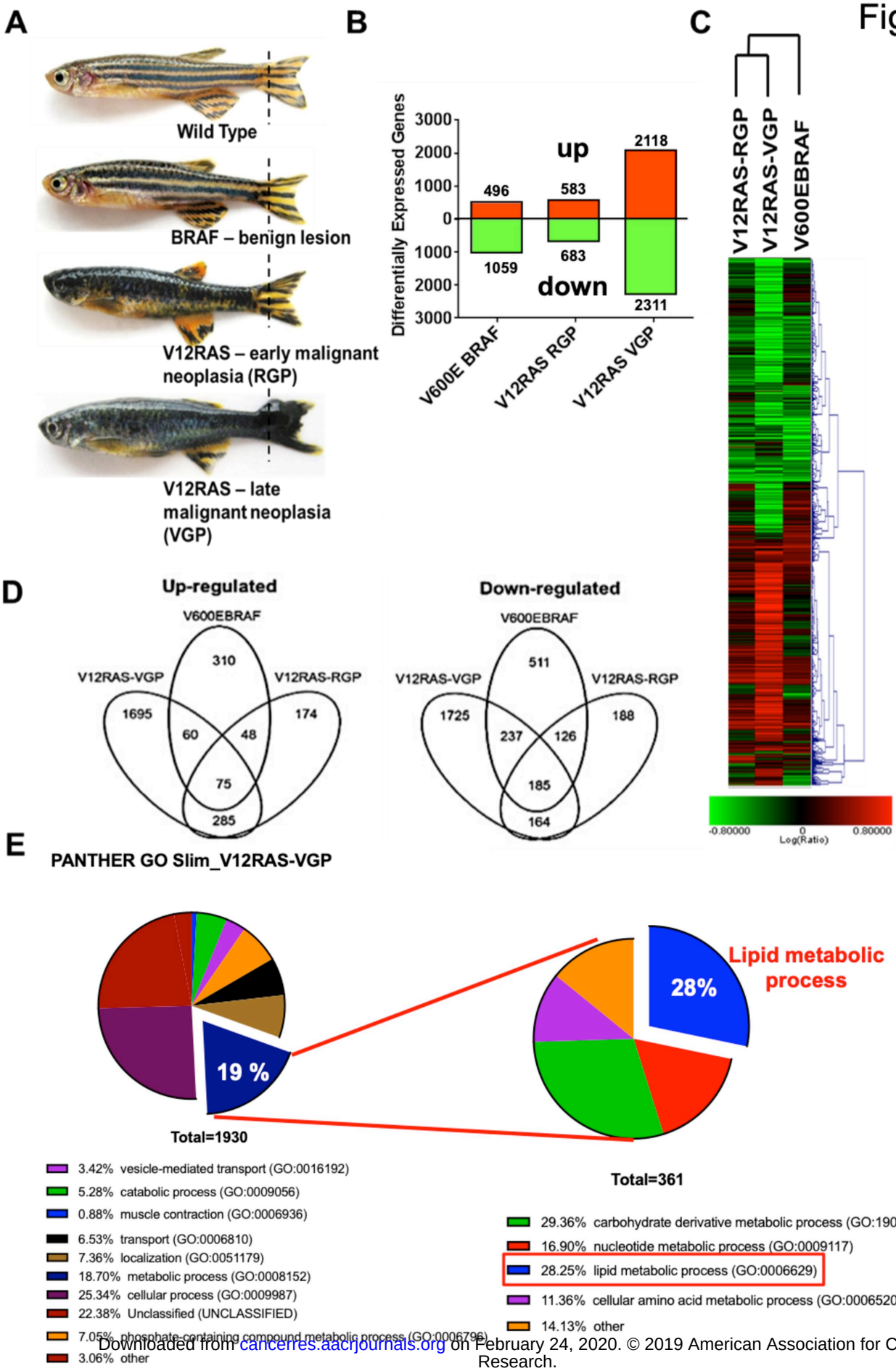

Figure 2

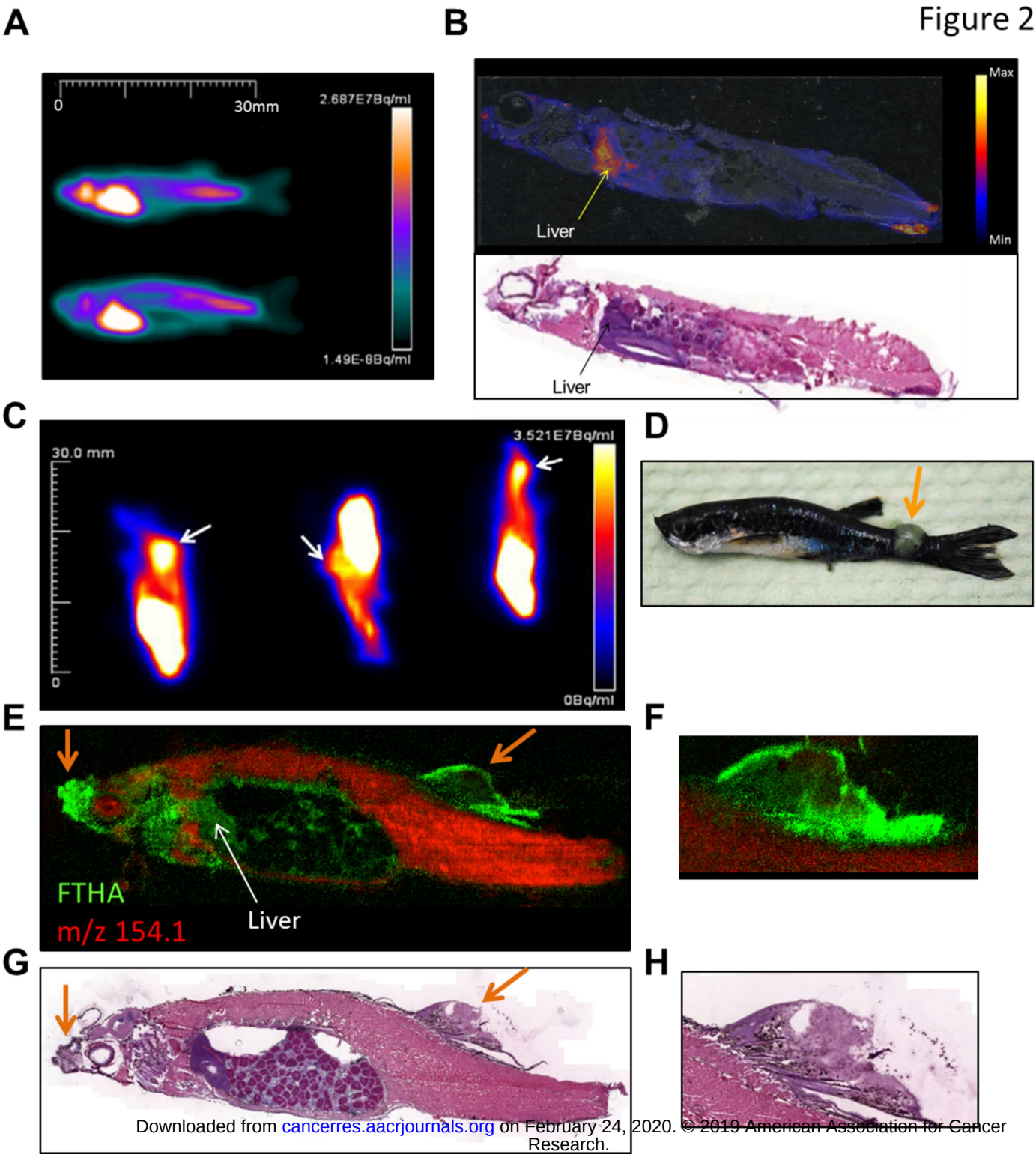

Figure 3

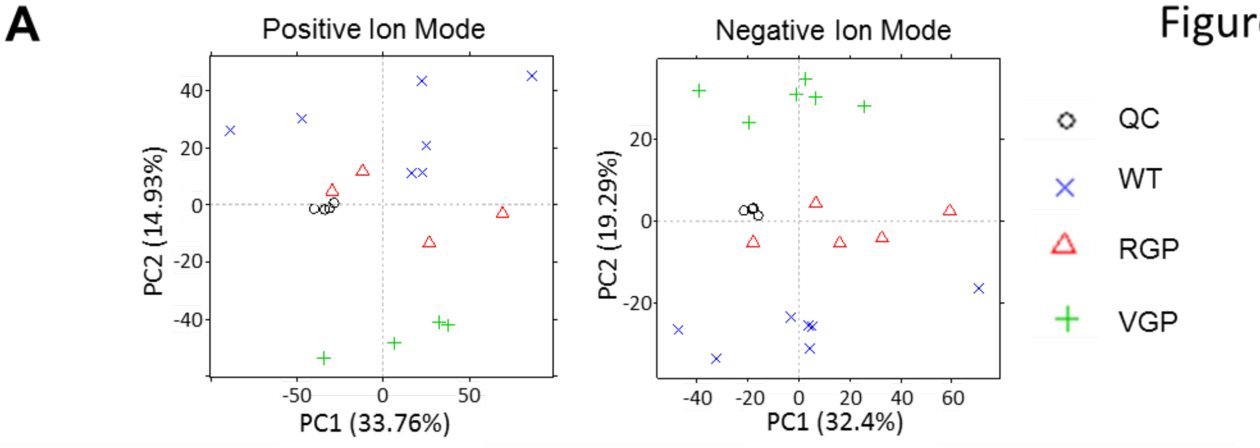

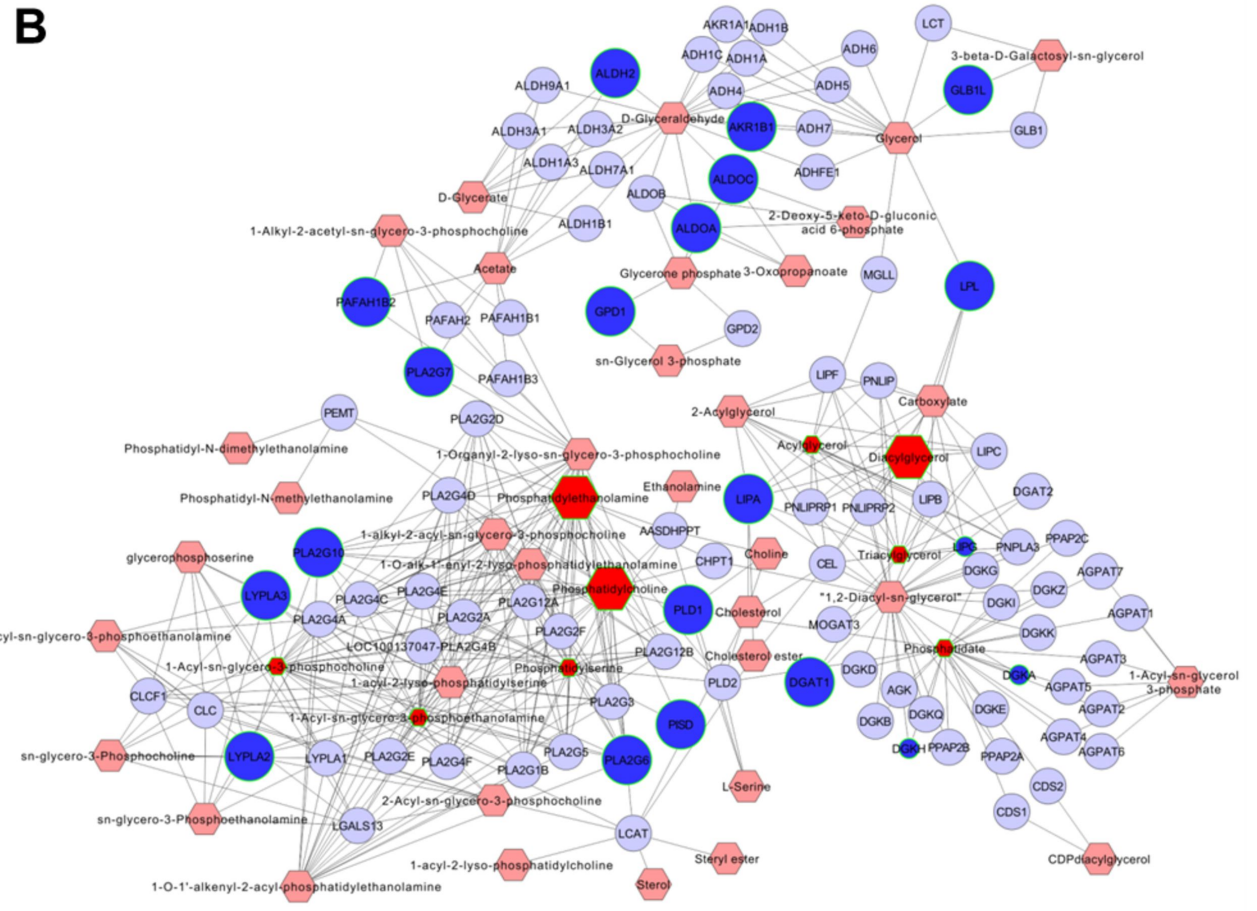

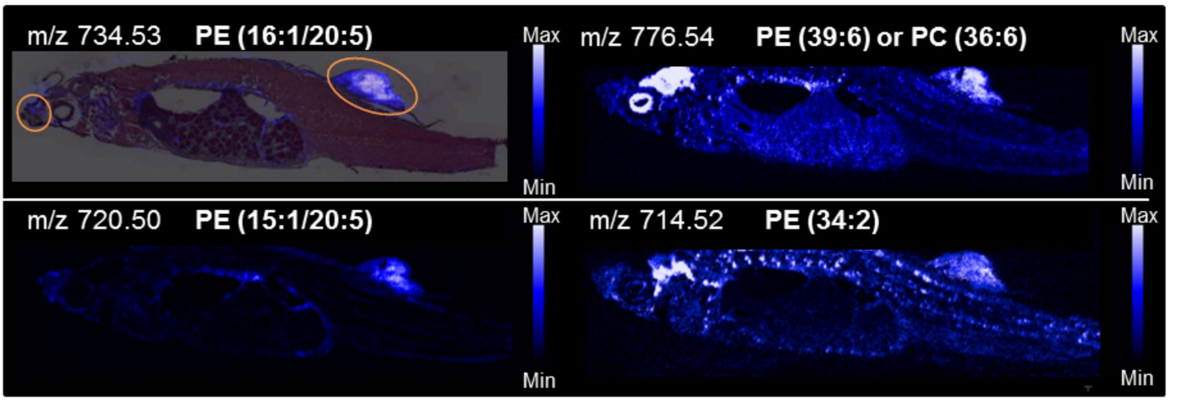

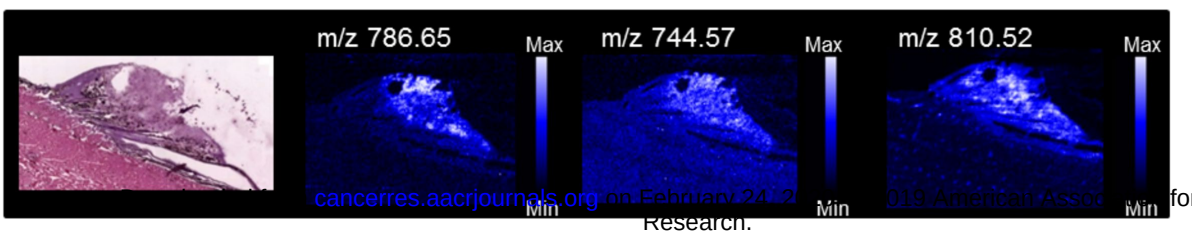

Figure 4

A

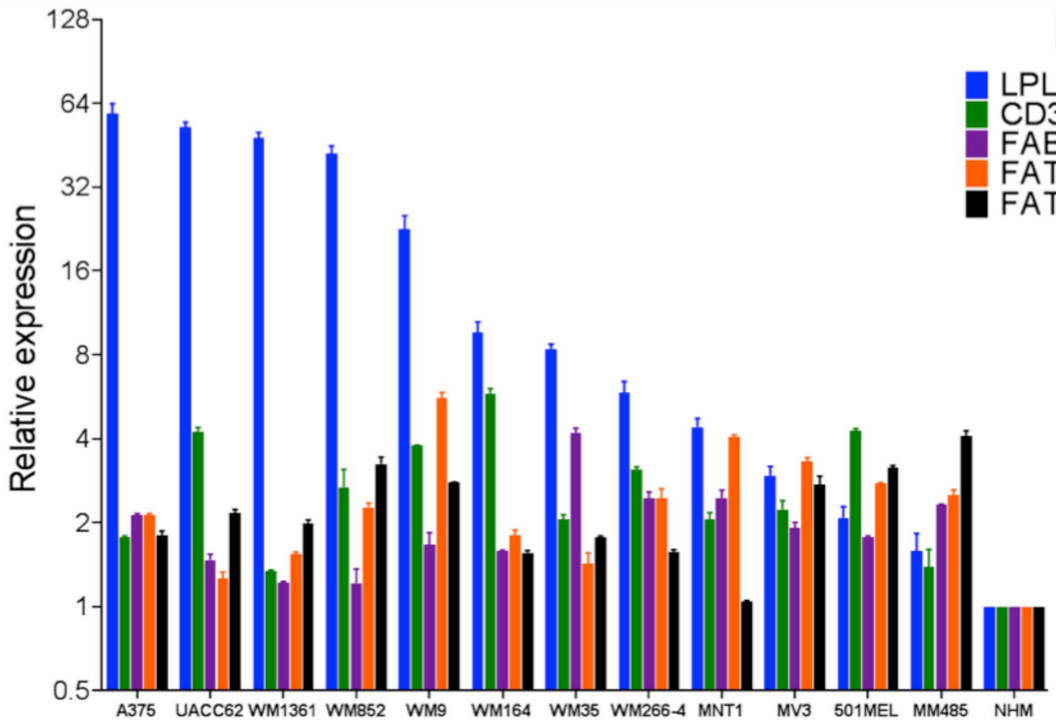

B

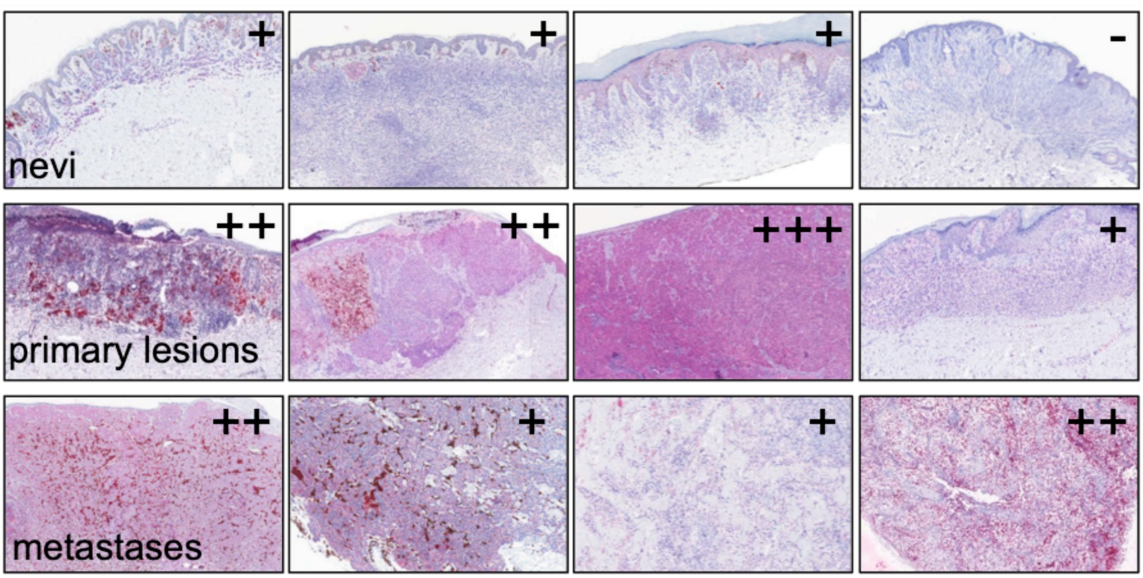

	LPL expression (% samples)			
	-	+	++	+++
Nevus (n=18)	23	67	10	0
Primary (n=21)	5	43	42	10
Metastasis (n= 8)	0	50	50	0

C

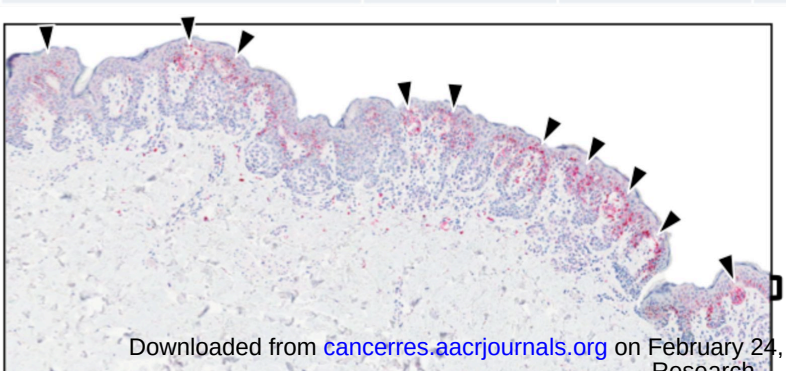

Figure 5

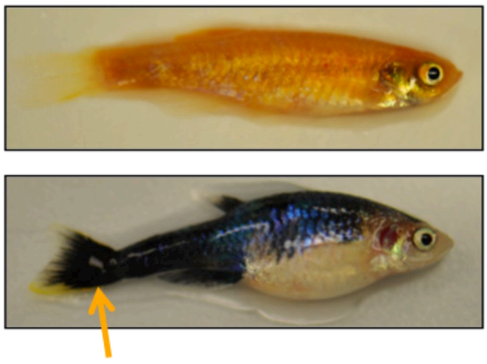

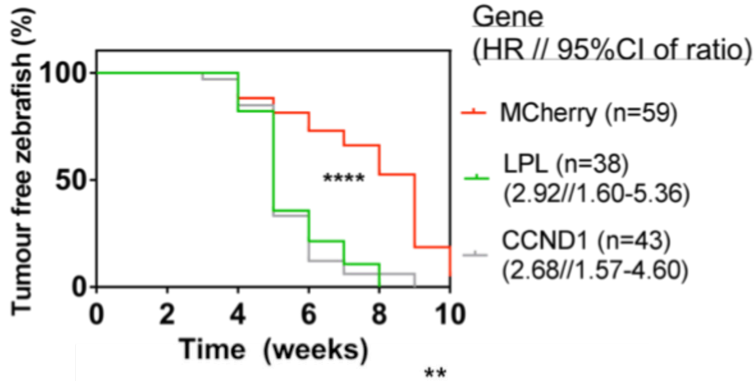

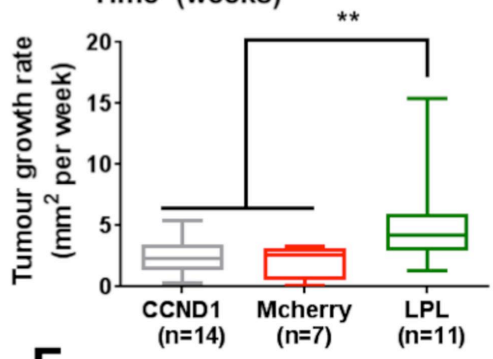

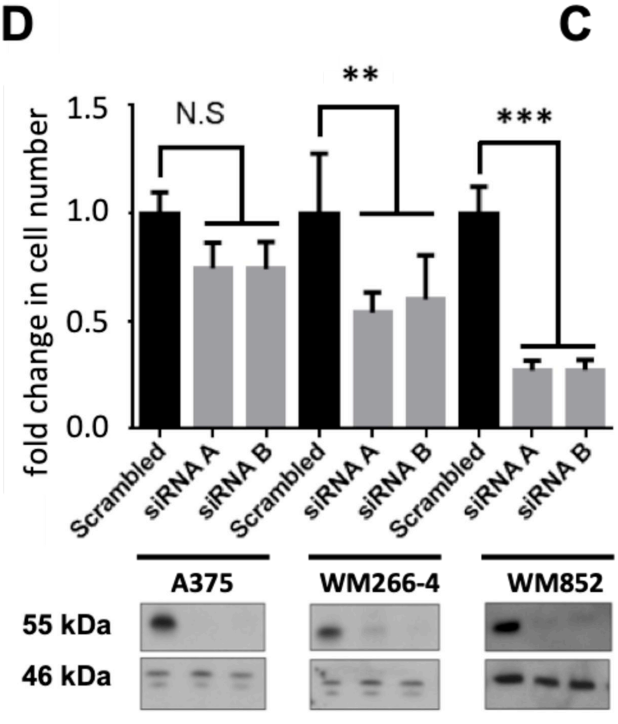

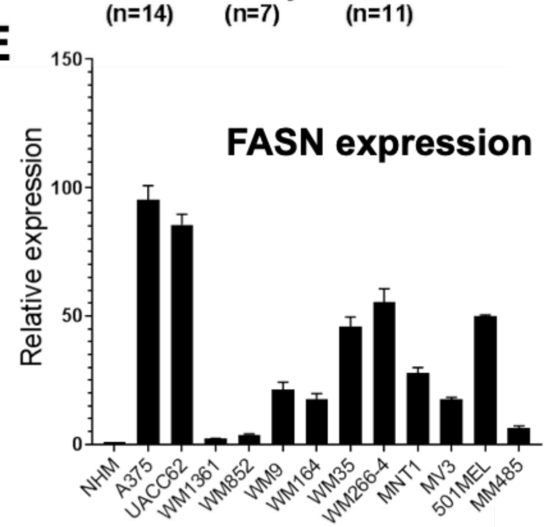

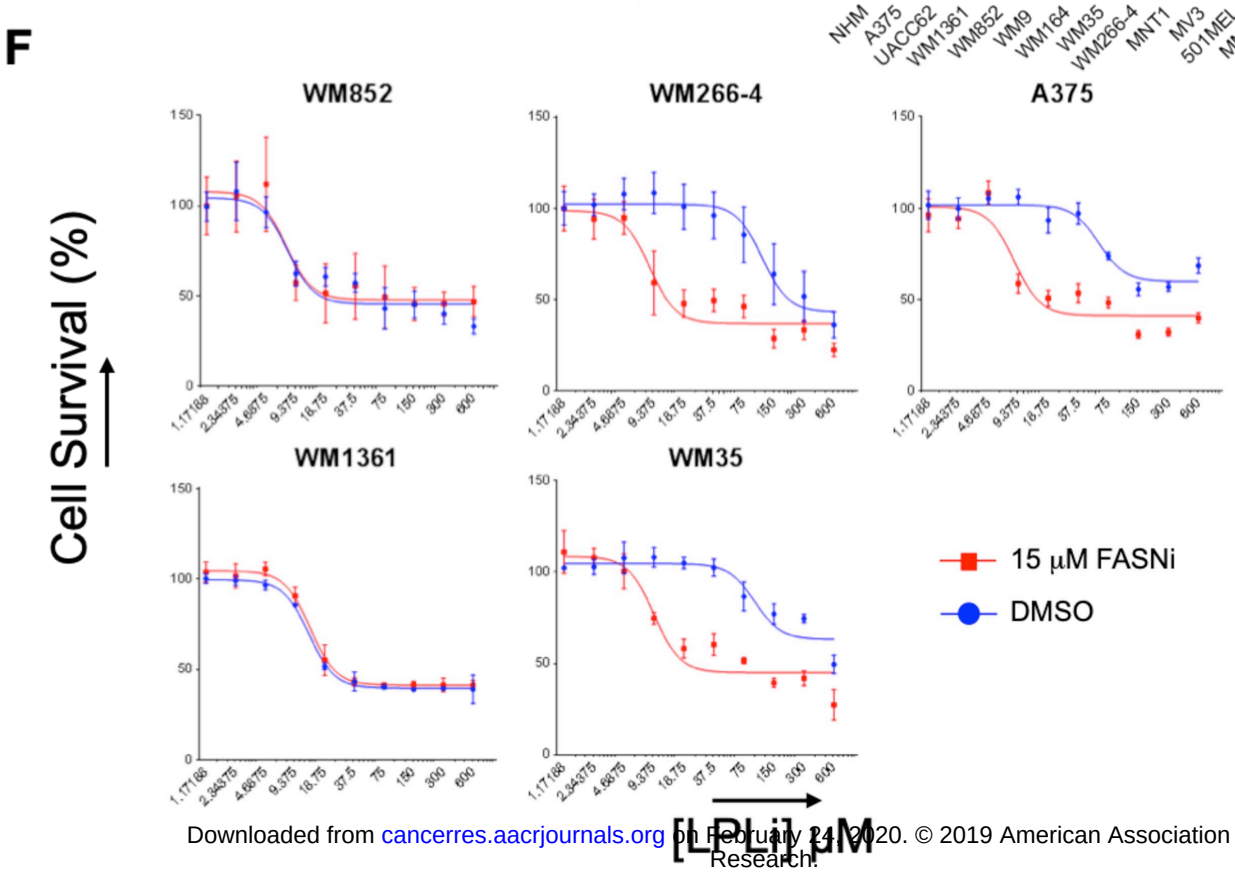

AACR American Association for Cancer Research

Cancer Research

The Journal of Cancer Research (1916–1930) | The American Journal of Cancer (1931–1940)

Enhanced fatty acid scavenging and glycerophospholipid metabolism accompanies melanocyte neoplasia progression in zebrafish

Fiona Henderson, Hannah R Johnston, Andrew P Badrock, et al.

Cancer Res Published OnlineFirst March 12, 2019.